



Simulating the generation of spin squeezing in a Rydberg atomic array for quantum metrology via a dissipative discrete truncated Wigner approximation

JINGYA WANG,¹ ZHONGXIAO XU,^{1,2} AND DONGHAO LI^{1,2,*}

¹State Key Laboratory of Quantum Optics and Quantum Optics Devices, Institute of Opto-electronics, Shanxi University, Taiyuan, Shanxi 030006, China

²Collaborative Innovation Center of Extreme Optics, Shanxi University, Taiyuan, Shanxi 030006, China

*lidonghao@sxu.edu.cn

Received 4 January 2023; revised 22 February 2023; accepted 27 February 2023; posted 28 February 2023; published 21 March 2023

An atomic ensemble with many-body entanglement is desirable for precision measurement. As a type of such quantum state, the spin squeezed state has been pursued in both cold and warm atoms for applications of a quantum-enhanced atomic clock, interferometer, and magnetometer. Here, we report the numerical simulation of many-body dynamics in a Rydberg atomic array with dipole–dipole interaction, and evaluate the generation of spin squeezing. The method builds on the dissipative discrete truncated Wigner approximation, which combines the mean-field dynamics of a spin ensemble with Monte Carlo sampling. By taking into account experimental imperfections such as spin decoherence, we apply this approach to the dynamics in both strontium and rubidium Rydberg atomic arrays with the current available scale. This offers the possibility to accurately simulate the many-body dynamics of interacting quantum systems in achievable platforms for application of quantum simulation and quantum metrology. © 2023 Optica Publishing Group

<https://doi.org/10.1364/JOSAB.484967>

1. INTRODUCTION

Many-body physics aims to understand matter with a collection of many interacting constituents. It connects different disciplines ranging from condensed-matter physics, statistics physics, to nuclear and high-energy physics. Although most of the complex quantum states were first discovered in solid-state materials, recent advances in highly controlled spin systems with long-range interactions including trapped ions [1,2], Rydberg atoms [3–6], and polar molecules [7–9] have greatly enhanced the prospects for probing exotic many-body phases of matter as well as for applications in quantum sensing and metrology, and provide opportunities to go beyond what is possible in real materials. Here, computational methods to model and benchmark large-scale spin systems play an essential role in unraveling fascinating aspects of the many-body problem on both theoretical and experimental sides.

Despite great progresses in computational techniques, the exponential growth in Hilbert space impedes scaling up calculations to reasonably sized systems, especially in higher dimensions. Specifically, as a widely used method in one-dimensional systems, the time-dependent density matrix renormalization group (tDMRG) method [10–12] is incompatible with the dynamics computation of high-dimensional

systems. On the other hand, a quantum many-body system out of equilibrium with long-range and strong interactions is prohibitive in numerical simulation with other techniques, such as perturbative techniques [13] and cluster expansions [14].

Aiming for entanglement-enhanced metrology such as an atomic clock and interferometer, here we use the dissipative discrete truncated Wigner approximation (DDTWA) [15] to numerically simulate the generation of spin squeezing in the spin–echo scheme through strong interaction between highly excited strontium and rubidium atoms with experimental imperfections. Similar to the route in DTWA [16], DDTWA applies the Monte Carlo sampling of discrete initial spin values to take account of the quantum fluctuation and correlation as shown in Figs. 1(a) and 1(b). In contrast to DTWA, stochastic trajectories are utilized to describe the dephasing and decay of atomic spin [17–20] instead of the coherent mean-field dynamics of classical spin variables [shown in Fig. 1(c)].

Surpassing the standard quantum limit is at the heart of quantum metrology. Advances in the field have led to the generation of entangled states such as spin squeezed states (SSSs) which can have reduced quantum uncertainty. Moreover, a SSS of atomic ensembles was suggested to be prepared for the improvement of

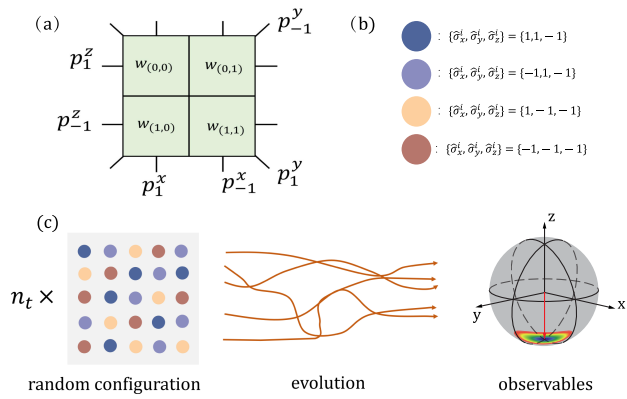


Fig. 1. (a) Discrete four-point Wigner quasiprobability distribution. The probability for a spin along $\pm x$, $\pm y$, and $\pm z$ directions can be described by sums over the vertical, diagonal, and horizontal lines, respectively. (b) Four configurations of initial spin along the $-z$ orientation. The initial spin vector is randomly drawn from one of the four configurations. (c) Process of simulation via the DTWA (DDTWA). (i) Monte Carlo sampling of initial spin vectors for N -particles atomic array. (ii) Time evolution of dynamics in light of classical equations of motion. (iii) The dynamic expectation of spin observables can be obtained by the statistical average of all trajectories undergoing time evolution.

sensitivity in atomic spectroscopy, magnetometers, interferometers, and atomic clocks. Several schemes have been proposed and demonstrated to generate such a SSS, including (1) the direct interaction of spins such as atomic collision in a Bose–Einstein condensate [21], (2) photon mediated spin–spin interaction in a cavity quantum electrodynamics system [22], and (3) quantum nondemolition measurement based conditional spin squeezing [23]. In this paper, we consider the first type, i.e., direct spin–spin interaction, realized by the strong van der Waals interactions between Rydberg atoms. To enable an experimentally available long coherence lifetime, an off-resonant coupling to the Rydberg state is adopted, leading to a long-range interaction $\sim 1/r^6$ between the atoms at a distance r within the atomic arrays.

We consider an atomic array consisting of N three-level atoms, as shown in Fig. 2(a1). In a ladder-type configuration, a laser beam drives the transition between the ground state $|g_i\rangle$ and excited state $|e_i\rangle$, and the associated Rabi frequency is given as Ω_1 . In addition, a second laser beam far-off-resonance by Δ coherently couples the excited state $|e_i\rangle$ to the Rydberg state $|r_i\rangle$ with Rabi frequency Ω_2 . Under the condition of far-off-resonance, the system can be effectively described as a two-level one with states $|g_i\rangle$ and $|\tilde{e}_i\rangle \sim |e_i\rangle - (\Omega_2/2\Delta)|r_i\rangle$, where $|\tilde{e}_i\rangle$ is the wave function from perturbation theory up to first order. Notably, here we use perturbation theory to treat atomic dynamics in the dressed state picture [$\otimes_k |e_k\rangle$, $|r_i r_j\rangle \otimes_{k \neq i, j} |e_k\rangle$] to determine the effective Rydberg–Rydberg atom interactions $V_{ij} = V_0 \frac{(R_c)^6}{|r_{ij}|^6 + (R_c)^6}$. The Hamiltonian of the atomic arrays becomes

$$H = \frac{\hbar\Omega_1}{2} \sum_i \hat{\sigma}_x^i + \sum_i \delta_i \hat{\sigma}_z^i + \sum_{i < j} V_{ij} \hat{\sigma}_z^i \hat{\sigma}_z^j \quad (\hbar = 1), \quad (1)$$

where $R_c = |C_6/(2\hbar\Delta)|^{1/6}$, $V_0 = (\Omega_2/2\Delta)^3 \hbar\Omega_2$, and $\delta_i = \delta_e + (1/2) \sum_{i \neq j} V_{ij}$, $\delta_e = -\Delta(1 - \sqrt{1 - 4(\Omega_2/2\Delta)^2})$

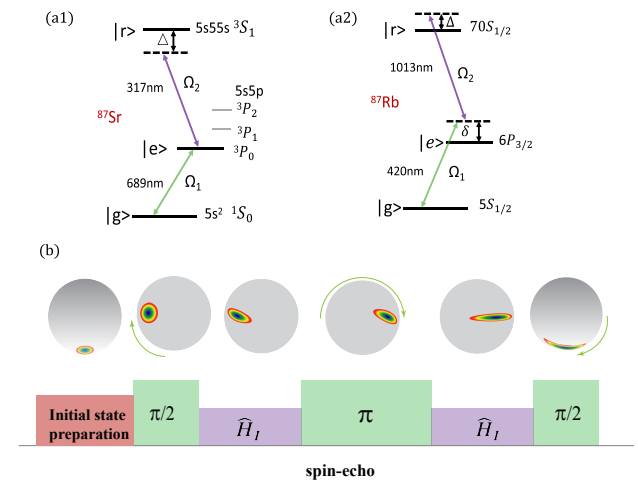


Fig. 2. (a) Schematic of energy levels for generating spin squeezing in Rydberg atomic array. The ground state $|g\rangle$ and high-lying Rydberg state $|r\rangle$ are coupled by two lasers through a mediate state $|e\rangle$. In the strontium atomic array (a1), the 689 nm laser resonantly couples $|g\rangle$ to the excited state $|e\rangle$ with Rabi frequency $\Omega_1 = 2\pi \times 0.02$ GHz. The 317 nm laser off-resonantly couples $|e\rangle$ to $|r\rangle$ with a detuning of $\Delta = 20\Omega_1$ and Rabi frequency $\Omega_2 = 2\pi \times 20$ MHz. In the rubidium atomic array (a2), the 420 nm laser couples $|e\rangle$ to $|r\rangle$ with Rabi frequency $\Omega_1 = 2\pi \times 60$ MHz and detuning $\delta = 2\pi \times 560$ MHz. The 1013 nm laser couples $|e\rangle$ to $|r\rangle$ with Rabi frequency $\Omega_2 = 2\pi \times 32$ MHz and detuning Δ . (b) Spin-echo scheme. A trail of pulses after the initial state preparation is applied to realize spin squeezing. The green pulses with different durations are the operation by the first laser. The purple pulses with the same duration are the operation by the second laser. The evolution of the spin state is depicted on the Bloch spheres.

is the light shift corresponding to the second process. r_{ij} is interatomic spacing, and $\sigma_x^i = |g_i\rangle\langle e_i| + |e_i\rangle\langle g_i|$, $\sigma_z^i = |e_i\rangle\langle e_i| - |g_i\rangle\langle g_i|$.

The signal-to-noise ratio seriously depends on the atomic number. Generally speaking, increasing the particle number of an atomic ensemble N is advantageous for precision measurements, since measurement precision is ultimately limited by the standard quantum limit (i.e., coherent spin state). However, the density number of cold atomic gas is much higher, but the available system size currently is limited to $10^3 \sim 10^4$ for atomic interferometry and optical lattice clocks. For instance, very recently Robinson *et al.* [26] and Pedrozo-Peñafiel *et al.* [27] demonstrated quantum-enhanced atomic clocks based on spin squeezing with $N \approx 19000$ and $N = 350 \pm 40$, respectively.

At present, ^{87}Sr and ^{87}Rb atom ensembles are the main platform of optical lattice clocks and atomic interferometry. Since SSSs are particularly suitable for improving the precision of atomic interferometry and optical lattice clocks, here we discuss the applications of spin squeezing on quantum-enhanced optical clocks and atomic interferometers based on ^{87}Sr and ^{87}Rb atomic arrays, respectively. In the following, we simulate the dynamics and generation of spin squeezing in realistic strontium and rubidium atomic arrays with DTWA and DDTWA, respectively. Specifically, the former can be applied in the entanglement-enhanced atomic clock, while the latter is a good candidate for a quantum-enhanced atomic interferometer.

2. SPIN SQUEEZING IN STRONTIUM ATOMIC ARRAY

Figure 2(a1) shows the energy levels involved in the interaction of strontium atoms. A two-photon transition between the ground state $|g\rangle$ ($|5s^2\ ^1S_0\rangle$) and a high-lying Rydberg state $|r\rangle$ ($|5s5s\ ^3S_1\rangle$) of a strontium atom is driven by two lasers. According to the experimentally achievable parameters [28], the first laser at 689 nm resonantly couples $|g\rangle$ to excited state $|e\rangle$ with Rabi frequency $\Omega_1 = 2\pi \times 0.02$ GHz. The second laser at 317 nm off-resonantly couples $|e\rangle$ ($|5s5p\ ^3P_0\rangle$) to the Rydberg state $|r\rangle$ with the detuning of $\Delta = 20\ \Omega_1$ and Rabi frequency $\Omega_2 = 2\pi \times 20$ MHz. Due to the narrow linewidth of $|e\rangle$ $\gamma^{-1} \gg T_{\text{int}}$ with the pulse operation time T_{int} , dephasing and decay can be safely neglected in the calculation. Consequently, we choose the DTWA technique, which combines sampling in discrete phase space with classical evolution under the mean-field approximation.

A spin-echo scheme [28] is used to be compatible with the application of quantum metrology, as illustrated in Fig. 2(b). Given the operation or pulse sequence, the detailed numerical simulation is performed by the following steps.

(1) **Initial state preparation.** We assume all atoms are populated in the ground state $|g\rangle$ by optical pumping. To take the initial quantum fluctuation or correlation into account, Monte Carlo sampling in phase space is applied. In general, any operator \hat{O} can be mapped to discrete phase space through the phase point operator $\hat{O}_\alpha^W = \text{Tr}[\hat{O}\hat{A}_\alpha]/2$ [29]. Regarding a single spin-1/2 particle, the phase point operator \hat{A}_α is given by

$$\hat{A}_\alpha = \hat{\rho}(r_\alpha) = (\hat{I} + r_\alpha \cdot \hat{\sigma})/2, \quad (2)$$

where $\alpha \in \{(0, 0), (0, 1), (1, 0), (1, 1)\}$, $r_{(0,0)} = (1, 1, 1)$, $r_{(0,1)} = (-1, -1, 1)$, $r_{(1,0)} = (1, -1, -1)$, $r_{(1,1)} = (-1, 1, -1)$, and $\hat{\sigma} = (\hat{\sigma}^x, \hat{\sigma}^y, \hat{\sigma}^z)$ are the usual Pauli operators. Similarly, the Wigner function w_α is the density operator map to phase space through the phase point operator. For the initial polarization in the ground state $|g\rangle$ aforementioned, the Wigner function is given by $w_{(1,0)} = w_{(1,1)} = 1/2$, and $w_{(0,0)} = w_{(0,1)} = 0$. This means that the probabilities for spin pointing along $-z$ and z directions are 100% and 0%, respectively. Similarly, the probabilities for a spin being in $\pm x$ and $\pm y$ directions are 50% and 50%, respectively. So the initial spin vectors are randomly drawn from one of the four configurations:

$$(\hat{\sigma}_x^i, \hat{\sigma}_y^i, \hat{\sigma}_z^i) = (\pm 1, \pm 1, -1). \quad (3)$$

(2) **$\pi/2$ rotation around x axis.** By applying a global $\pi/2$ optical pulse around the x axis at 689 nm to the atoms, the total spin vector in the Bloch sphere rotates from the initial $-z$ direction to the y direction. The effective interaction takes the form of $\hat{H}_I = \frac{1}{2}\hbar\Omega_1\hat{\sigma}_x^i$, leading to the corresponding classical equations of motion as

$$\dot{\hat{\sigma}}_x^i = 0, \quad (4)$$

$$\dot{\hat{\sigma}}_y^i = -\Omega_1\hat{\sigma}_z^i, \quad (5)$$

$$\dot{\hat{\sigma}}_z^i = \Omega_1\hat{\sigma}_y^i. \quad (6)$$

(3) **Spin squeezing through spin-spin interaction.** By switching on the far-off-resonance at 317 nm solely with a duration of $t/2$, the interaction $\hat{H}_I = \sum_{i \neq j}^N V_{ij}\hat{\sigma}_z^i\hat{\sigma}_z^j$ between Rydberg atoms is realized, which leads to a one-axis twisting of the uncertainty ellipse. The corresponding classical equations of motion are

$$\dot{\hat{\sigma}}_x^i = -\sum_{j \neq i} V_{ij}\hat{\sigma}_y^i\hat{\sigma}_z^j, \quad (7)$$

$$\dot{\hat{\sigma}}_y^i = \sum_{j \neq i} V_{ij}\hat{\sigma}_x^i\hat{\sigma}_z^j, \quad (8)$$

$$\dot{\hat{\sigma}}_z^i = 0, \quad (9)$$

where $V_0 = 2$ kHz, blockade radius $R_c = 5a$, and a is the distance between the nearest neighboring atoms. We numerically integrate the equations of motion using a fourth-order Runge-Kutta method.

(4) **π rotation around x axis.** To eliminate the broadening caused by δ_i , we apply a π pulse to rotate the total spin vector in the Bloch by 180° along the x axis.

(5) **Mirror operation of steps (2) and (3).** By implementing the $t/2$ -duration spin squeezing and a global $\pi/2$ rotation around the x axis successively, a spin-echo scheme is accomplished with a reduction of spin variance in the final population measurement. The corresponding classical equations of motion are similar to those in steps (2) and (3).

Given the $n_t \gg 1$ Monte Carlo sampling for the initial states, the dynamic expectation values of spin observables are calculated from the average over all trajectories.

Consider a collective atomic spin given by the sum of the total angular momenta of individual atoms, $\hat{s}_i = \sum_k \hat{\sigma}_i^k$, with $i = x, y, z$. One can finally evaluate the spin squeezing through the squeezing parameter [30] $\xi^2 = \frac{N(\Delta s_{\perp, \min})^2}{\langle s \rangle^2}$, where $\Delta s_{\perp, \min}$ is the minimum variance in the plane perpendicular to the mean total spin vector $\langle s \rangle$. It is found that the measured macroscopic spin orients along the z axis, and the mean spin $\langle s_x \rangle = \langle s_y \rangle = 0$. The perpendicular spin component is thus $\hat{s}_{\perp}(\theta) = \cos(\theta)\hat{s}_x + \sin(\theta)\hat{s}_y$, with the relative angle θ to the x axis, and the associated uncertainty is expressed as

$$(\Delta \hat{s}_{\perp})^2 = \cos^2(\theta) \langle \hat{s}_x^2 \rangle + \sin^2(\theta) \langle \hat{s}_y^2 \rangle + \cos(\theta) \sin(\theta) \langle \hat{s}_x \hat{s}_y + \hat{s}_y \hat{s}_x \rangle. \quad (10)$$

Intuitively, the larger n_t gives the better results, approaching real values; however, the optimization of the computational resources should be taken into account. Here we calculate the optimal squeezing with different numbers of trajectories n_t in a 32×32 atomic array. In Fig. 3, the results converge with an exact solution as the increasing number of sample trajectories n_t (the error is 0.09 dB for $n_t = 1000$). By balancing the computation time and accuracy, we fix $n_t = 1000$ in the following numerical simulation.

In Fig. 4, we plot the time evolution of the squeezing parameter for $N = 5 \times 5$ and 16×16 , which shows that the numerical simulation results are in agreement with the exact results. In

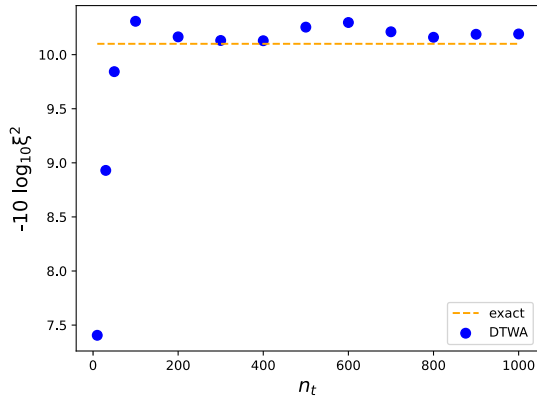


Fig. 3. Spin squeezing parameter ξ^2 as a function of the number of sample trajectories n_t . The result converges on the exact solution as the increasing number of n_t . The blue dots and dashed line denote the results of the DTWA and the exact solution of $N = 32 \times 32$, respectively.

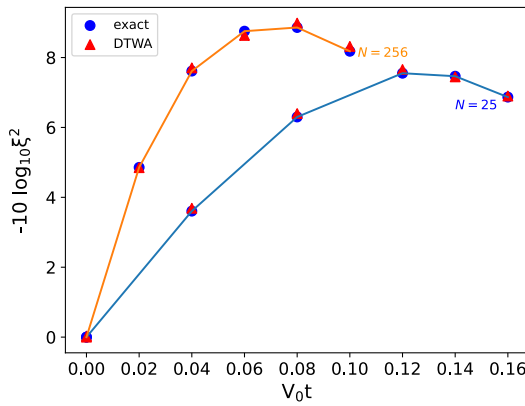


Fig. 4. Time evolution of the spin squeezing parameter ξ^2 . The result of DTWA is in good agreement with the exact solution for the different sizes of the strontium atomic array. The blue (orange) curve represents the trendline of the squeezing parameter for $N = 5 \times 5$ ($N = 16 \times 16$). The solid blue circles and red triangles denote the results of the exact solution and the DTWA, respectively. The lines are to guide the eye.

addition, we evaluated optimal squeezing parameter $\xi^2 = 0.095$ for $N = 32 \times 32$. With the increase of N , the optimal squeezing is improved, suggesting entanglement is not limited by the interaction range and can spread with the increase of system size.

3. SPIN SQUEEZING IN RUBIDIUM ATOMIC ARRAY

Although numerical simulation of the complex quantum spin system has enormous advantages, DTWA is not suitable for an open system with dissipation. To overcome this limit, we make use of the DDTWA method by adding a random term related to dissipation in the evolutionary process.

We consider N -particles two-dimensional ^{87}Rb atomic arrays [31–33] by using the experimental parameter in Ref. [34]. As shown in Fig. 2(a2), we couple the ground state $|g\rangle$ ($|5S_{1/2}, F = 2, m_F = -2\rangle$) to the Rydberg state $|r\rangle$ ($|70S_{1/2}, J = 1/2,$

$m_J = -1/2\rangle$) mediated by an excited state $|e\rangle$ ($|6P_{3/2}, F = 3, m_F = -3\rangle$) through a two-photon process. Transitions between $|g\rangle$ and excited state $|e\rangle$ are laser-driven with Rabi frequency $\Omega_1 = 2\pi \times 60$ MHz and detuning $\delta = 2\pi \times 560$ MHz. Transitions between $|e\rangle$ and $|r\rangle$ are driven by the second laser at 1013 nm with Rabi frequency $\Omega_2 = 2\pi \times 32$ MHz and detuning $\Delta = 2\pi \times 0.8$ MHz. A blockade radius is $R_c = 3a$ with the distance between the nearest neighboring atoms $a = 2.87 \mu\text{m}$, and $V_0 = 2\pi \times 2$ MHz [34]. The 70S Rydberg state has a lifetime of $\tau = 150 \mu\text{s}$ and the intermediate state has a lifetime of $50 \mu\text{s}$.

This open system can be modeled by the rotating wave quantum Langevin equation [35]

$$\begin{aligned} \dot{O} = & i[H, O] - [O, C^\dagger] \left(\frac{\Gamma}{2} C + \sqrt{\Gamma} \hat{f}(t) \right) \\ & - \left(\frac{\Gamma}{2} C^\dagger + \sqrt{\Gamma} \hat{f}^\dagger(t) \right) [C, O], \end{aligned} \quad (11)$$

where O is a system operator, Γ is decay rate, jump operator $C = \sigma^- = \frac{1}{2}(\sigma_x - i\sigma_y)$, and \hat{f} is the quantum noise operator.

Similar to the strontium atomic array, a spin-echo scheme is used to generate the SSS of the ^{87}Rb atomic array, as shown in Fig. 2(a2). However, the coherent mean-field dynamics of the classical spin variables is replaced by stochastic trajectories to describe the dissipation. Concretely, regarding step (2), the increments for the classical spin trajectories are written as

$$d\sigma_x^i = d\sigma_x^i|_{\text{decay}} dt, \quad (12)$$

$$d\sigma_y^i = (-\Omega_1 \sigma_z^i + d\sigma_y^i|_{\text{decay}}) dt, \quad (13)$$

$$d\sigma_z^i = (\Omega_1 \sigma_y^i + d\sigma_z^i|_{\text{decay}}) dt. \quad (14)$$

For step (3), the increments for the classical spin trajectories are

$$d\sigma_x^i = \left(-\sum_{i \neq j} V_{ij} \sigma_y^i \sigma_z^j + d\sigma_x^i|_{\text{decay}} \right) dt, \quad (15)$$

$$d\sigma_y^i = \left(\sum_{i \neq j} V_{ij} \sigma_x^i \sigma_z^j + d\sigma_y^i|_{\text{decay}} \right) dt, \quad (16)$$

$$d\sigma_z^i = d\sigma_z^i|_{\text{decay}} dt. \quad (17)$$

Equations (12)–(17) are deterministic describing the coherent interaction, while $d\hat{\sigma}_x^i|_{\text{decay}}, d\hat{\sigma}_y^i|_{\text{decay}}, d\hat{\sigma}_z^i|_{\text{decay}}$ introduce the spin fluctuation to preserve the length of each spin $d\hat{s}_i^2|_{\text{decay}} = 0$ [15]. This set of equations can be efficiently simulated numerically with the Euler–Maruyama method [36]. So we obtain

$$d\sigma_x^i|_{\text{decay}} = -\frac{\Gamma}{2} \sigma_x^i dt - \sqrt{\Gamma} \sigma_y^i \xi_i(t) dt, \quad (18)$$

$$d\sigma_y^i|_{\text{decay}} = -\frac{\Gamma}{2} \sigma_y^i dt - \sqrt{\Gamma} \sigma_x^i \xi_i(t) dt, \quad (19)$$

$$d\sigma_z^i|_{\text{decay}} = -\Gamma(\sigma_z^i + 1)dt + \sqrt{\Gamma}(\sigma_z^i + 1)\xi_i(t)dt, \quad (20)$$

where $\Gamma = 1/\tau$ is the uncorrelated decay rate of each spin. ξ_i is independent noise processes, and the increment is a random number extracted from the standard normal distribution. Consequently, the spin squeezing parameter is calculated from the average over all trajectories. In Fig. 5, we show the time evolution of the squeezing parameter. For $N = 16 \times 16$ and 32×32 , the optimal squeezings are 8.1817 dB and 9.498 dB, respectively.

We proceed to analyze the influence of the variation of Rabi frequency as well as two-photon detuning in an ^{87}Rb array with $N = 16 \times 16$ via the Monte Carlo sampling. In particular, we add a fluctuation term β [37] with mean value as zero; thus the associated total Rabi frequency and two-photon detuning are $(1 + \beta)\Omega$ and $(1 + \beta)\Delta$, respectively. In the sampling, β has been randomly drawn from a normal distribution (mean value $\mu = 0$, standard deviation σ) with the sample trajectories, $n_t = 2000$. As shown in Fig. 6, the effect of detuning fluctuation on optimal squeezing is slightly greater than that of the Rabi frequency, and the optimal squeezing degrades rapidly with increasing the fluctuation amplitude of Rabi frequency.

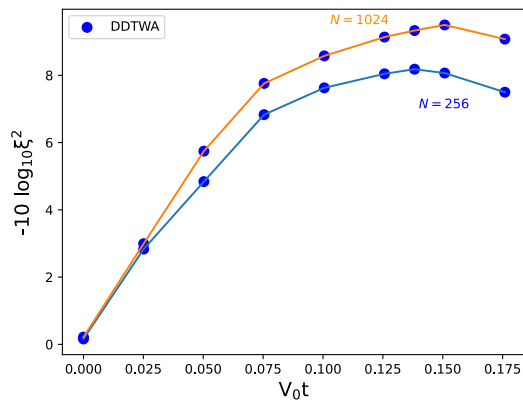


Fig. 5. Time evolution of the spin squeezing parameter ξ^2 via the method of DDTWA in the rubidium atomic array. For the ensembles of $N = 16 \times 16$ and 32×32 , the optimal squeezings are 8.1817 dB and 9.498 dB, respectively. The lines are to guide the eye.

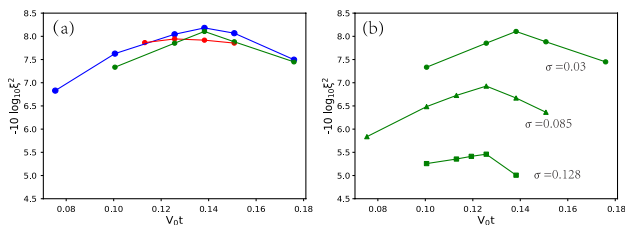


Fig. 6. Time evolution of the spin squeezing parameter ξ^2 under Rabi frequency and detuning in different error fractions β . (a) The blue dots are the results without any fluctuation, i.e., $\sigma = 0$. The effect of detuning fluctuation (red dots) on optimal squeezing is slightly greater than that of the Rabi frequency (green dots). The error fraction β is drawn from a normal distribution (mean value $\mu = 0$, standard deviation $\sigma = 0.03$). (b) Optimal squeezing with different amplitudes of Rabi frequency fluctuation. The lines are to guide the eye.

4. CONCLUSION

To conclude, we report the numerical simulation of generating SSSs in atomic arrays via strong van der Waals interactions between Rydberg atoms. In regard of the experimental feasibility and imperfection, the methods of DTWA and DDTWA are exploited to deal with the two-dimensional strontium and rubidium atomic arrays, respectively. In particular, due to the nonnegligible dissipation in the rubidium atomic system, stochastic trajectories are employed to include the exchange between the system and the surrounding environment. Our results can be directly used for applications of quantum-enhanced metrology, such as atomic clocks and interferometers. This technique offers the possibilities to simulate large-scale quantum many-body systems with tunable range interactions, and also can be easily extended to high-dimensional models.

Funding. National Key Research and Development Program of China (2020YFA0309400); Shanxi Provincial Key Research and Development Project (202101150101025); National Natural Science Foundation of China (11974228, 12174081, 12204289, 12222409).

Disclosures. The authors declare no conflicts of interest.

Data availability. Data underlying the results presented in this paper are not publicly available at this time but may be obtained from the authors upon reasonable request.

REFERENCES

- R. Islam, C. Senko, W. C. Campbell, S. Korenblit, J. Smith, A. Lee, E. E. Edwards, C.-C. J. Wang, J. K. Freericks, and C. Monroe, "Emergence and frustration of magnetism with variable-range interactions in a quantum simulator," *Science* **340**, 583–587 (2013).
- P. Richerme, Z.-X. Gong, A. Lee, C. Senko, J. Smith, M. Foss-Feig, S. Michalakakis, A. V. Gorshkov, and C. Monroe, "Non-local propagation of correlations in long-range interacting quantum systems," *Nature* **511**, 198–201 (2014).
- I. S. Madjarov, J. P. Covey, A. L. Shaw, J. Choi, A. Kale, A. Cooper, H. Pichler, V. Schkolnik, J. R. Williams, and M. Endres, "High-fidelity entanglement and detection of alkaline-earth Rydberg atoms," *Nat. Phys.* **16**, 857–861 (2020).
- A. Browaeys and T. Lahaye, "Many-body physics with individually controlled Rydberg atoms," *Nat. Phys.* **16**, 132–142 (2020).
- P. Scholl, M. Schuler, H. J. Williams, A. A. Eberharter, D. Barredo, K.-N. Schymik, V. Lienhard, L.-P. Henry, T. C. Lang, T. Lahaye, A. M. Läuchli, and A. Browaeys, "Quantum simulation of 2D antiferromagnets with hundreds of Rydberg atoms," *Nature* **595**, 233–238 (2021).
- S. Ebadi, T. T. Wang, H. Levine, A. Keesling, G. Semeghini, A. Omran, D. Bluvstein, R. Samajdar, H. Pichler, W. W. Ho, S. Choi, S. Sachdev, M. Greiner, V. Vuletić, and M. D. Lukin, "Quantum phases of matter on a 256-atom programmable quantum simulator," *Nature* **595**, 227–232 (2021).
- J. L. Bohn, A. M. Rey, and J. Ye, "Cold molecules: Progress in quantum engineering of chemistry and quantum matter," *Science* **357**, 1002–1010 (2017).
- B. Yan, S. Moses, B. Gadway, J. Covey, K. Hazzard, A. Rey, D. Jin, and J. Ye, "Observation of dipolar spin-exchange interactions with lattice-confined polar molecules," *Nature* **501**, 521–525 (2013).
- K. R. A. Hazzard, B. Gadway, M. Foss-Feig, B. Yan, S. A. Moses, J. P. Covey, N. Y. Yao, M. D. Lukin, J. Ye, D. S. Jin, and A. M. Rey, "Many-body dynamics of dipolar molecules in an optical lattice," *Phys. Rev. Lett.* **113**, 195302 (2014).
- G. Vidal, "Efficient simulation of one-dimensional quantum many-body systems," *Phys. Rev. Lett.* **93**, 040502 (2004).
- S. R. White and A. E. Feiguin, "Real-time evolution using the density matrix renormalization group," *Phys. Rev. Lett.* **93**, 076401 (2004).

12. A. J. Daley, C. Kollath, U. Schollwöck, and G. Vidal, "Time-dependent density-matrix renormalization-group using adaptive effective Hilbert spaces," *J. Stat. Mech. Theory Exp.* **2004**, P04005 (2004).
13. A. H. Nayfeh, *Introduction to Perturbation Techniques* (Wiley, 2011).
14. J. M. Sanchez, "Cluster expansions and the configurational energy of alloys," *Phys. Rev. B* **48**, 14013–14015 (1993).
15. J. Huber, A. M. Rey, and P. Rabl, "Realistic simulations of spin squeezing and cooperative coupling effects in large ensembles of interacting two-level systems," *Phys. Rev. A* **105**, 013716 (2022).
16. J. Schachenmayer, A. Pikovski, and A. M. Rey, "Many-body quantum spin dynamics with monte carlo trajectories on a discrete phase space," *Phys. Rev. X* **5**, 011022 (2015).
17. R. Orús and G. Vidal, "Infinite time-evolving block decimation algorithm beyond unitary evolution," *Phys. Rev. B* **78**, 155117 (2008).
18. E. Mascarenhas, H. Flayac, and V. Savona, "Matrix-product-operator approach to the nonequilibrium steady state of driven-dissipative quantum arrays," *Phys. Rev. A* **92**, 022116 (2015).
19. J. Cui, J. I. Cirac, and M. C. Bañuls, "Variational matrix product operators for the steady state of dissipative quantum systems," *Phys. Rev. Lett.* **114**, 220601 (2015).
20. H. Weimer, A. Kshetriamayam, and R. Orús, "Simulation methods for open quantum many-body systems," *Rev. Mod. Phys.* **93**, 015008 (2021).
21. O. Morsch and M. Oberthaler, "Dynamics of Bose-Einstein condensates in optical lattices," *Rev. Mod. Phys.* **78**, 179–215 (2006).
22. P. Samutpraphoot, T. Đorđević, P. L. Ocola, H. Bernien, C. Senko, V. Vuletić, and M. D. Lukin, "Strong coupling of two individually controlled atoms via a nanophotonic cavity," *Phys. Rev. Lett.* **124**, 063602 (2020).
23. H. Bao, J. Duan, S. Jin, X. Lu, P. Li, W. Qu, M. Wang, I. Novikova, E. E. Mikhailov, K.-F. Zhao, K. Mølmer, H. Shen, and Y. Xiao, "Spin squeezing of 1011 atoms by prediction and retrodiction measurements," *Nature* **581**, 159–163 (2020).
24. J. E. Johnson and S. L. Rolston, "Interactions between Rydberg-dressed atoms," *Phys. Rev. A* **82**, 033412 (2010).
25. R.-H. Zheng, S.-L. Su, J. Song, W. Li, and Y. Xia, "Thermal-dephasing-tolerant generation of Schrodinger cat states with Rydberg dressed blockade," *arXiv*, arXiv:2301.05389 (2023).
26. J. M. Robinson, M. Miklos, Y. M. Tso, C. J. Kennedy, D. Kedar, J. K. Thompson, and J. Ye, "Direct comparison of two spin squeezed optical clocks below the quantum projection noise limit," *arXiv*, arXiv:2211.08621 (2022).
27. E. Pedrozo-Peñañiel, S. Colombo, C. Shu, A. F. Adiyatullin, Z. Li, E. Mendez, B. Braverman, A. Kawasaki, D. Akamatsu, Y. Xiao, and V. Vuletić, "Entanglement on an optical atomic-clock transition," *Nature* **588**, 414–418 (2020).
28. L. I. R. Gil, R. Mukherjee, E. M. Bridge, M. P. A. Jones, and T. Pohl, "Spin squeezing in a Rydberg lattice clock," *Phys. Rev. Lett.* **112**, 103601 (2014).
29. W. K. Wootters, "A Wigner-function formulation of finite-state quantum mechanics," *Ann. Phys., NY* **176**, 1–21 (1987).
30. D. J. Wineland, J. J. Bollinger, W. M. Itano, F. L. Moore, and D. J. Heinzen, "Spin squeezing and reduced quantum noise in spectroscopy," *Phys. Rev. A* **46**, R6797–R6800 (1992).
31. D. Barredo, S. de Léséleuc, V. Lienhard, T. Lahaye, and A. Browaeys, "An atom-by-atom assembler of defect-free arbitrary two-dimensional atomic arrays," *Science* **354**, 1021–1023 (2016).
32. M. Endres, H. Bernien, A. Keesling, H. Levine, E. R. Anschuetz, A. Krajenbrink, C. Senko, V. Vuletic, M. Greiner, and M. D. Lukin, "Atom-by-atom assembly of defect-free one-dimensional cold atom arrays," *Science* **354**, 1024–1027 (2016).
33. H. Kim, W. Lee, H.-G. Lee, H. Jo, Y. Song, and J. Ahn, "In situ single-atom array synthesis using dynamic holographic optical tweezers," *Nat. Commun.* **7**, 13317 (2016).
34. H. Bernien, S. Schwartz, A. Keesling, H. Levine, A. Omran, H. Pichler, S. Choi, A. S. Zibrov, M. Endres, M. Greiner, V. Vuletić, and M. D. Lukin, "Probing many-body dynamics on a 51-atom quantum simulator," *Nature* **551**, 579–584 (2017).
35. W. P. Bowen and G. J. Milburn, *Quantum Optomechanics* (CRC Press, 2015).
36. C. Gardiner, *Stochastic Methods* (Springer, 2009).
37. L.-N. Sun, L.-L. Yan, S.-L. Su, and Y. Jia, "One-step implementation of time-optimal-control three-qubit nonadiabatic holonomic controlled gates in Rydberg atoms," *Phys. Rev. Appl.* **16**, 064040 (2021).